Acta Geochim (2022) 41(1):64–83
https://doi.org/10.1007/s11631-021-00496-w

ORIGINAL ARTICLE

Geochemistry of metasedimentary rocks of the Sonakhan and Mahakoshal greenstone belts, Central India: Implications for paleoweathering, paleogeography and mechanisms of greenstone belt development

Hamidullah Wani[1] · M. E. A. Mondal[2] · Iftikhar Ahmad[2]

Received: 27 February 2021 / Revised: 23 July 2021 / Accepted: 31 August 2021 / Published online: 25 September 2021
© Science Press and Institute of Geochemistry, CAS and Springer-Verlag GmbH Germany, part of Springer Nature 2021

Abstract A comparative study of the Precambrian Sonakhan (SGB) and Mahakoshal (MGB) greenstones belts of Central India has been undertaken to decipher their provenance, paleoweathering, paleogeography, and tectonics. As compared to the Upper Continental Crust (UCC), the MGB samples are enriched while the SGB samples are depleted in mafic elements indicating the presence of mafic rocks in the source of the MGB. This is complemented by the Ni–Cr diagram. The REE concentrations, LREE fractionated patterns and negative Eu anomalies of the MGB and SGB samples indicate derivation of sediments from a highly fractionated granitic source. Since MGB samples also contain the geochemical signature of mafic rocks, it is, therefore proposed that the MGB clastic load were derived from two sources (mafic + felsic) with arc character. This is attested by Cr and Zr relationships, and LILE enrichment, and HFSE depletion. These features suggest that the SGB developed as autochthonous while the MGB developed as an allochthonous belt. The chemical alteration indices such as chemical index of alteration (CIA), plagioclase index of alteration (PIA), and index of compositional variability for MGB samples indicate that they were dominantly derived as the first cycle (with minor recycled) sediments from bimodal sources (dominantly continental arcs) by intense chemical weathering as compared to the SGB samples, which were derived from felsic sources (dominantly cratonic rocks), and partly by recycling through a low chemical weathering. The CIA and PIA values of the samples reveal a change in the climatic conditions from Late Archean to Late Paleoproterozoic. Such change is interpreted in terms of migration of the Indian plate from high latitudes in the Late Archean to lower latitudes during the Late Paleoproterozoic. This is consistent with the paleomagnetic data that placed India in the configuration of 2.45 Ga Ur and 1.78 Ga Columbia supercontinents.

Keywords Central Indian Shield · Sonakhan and Mahakoshal greenstone belts · Paleoweathering and paleogeography · Greenstone belt development

Abbreviations

SGB	Sonakhan greenstone belt
MGB	Mahakoshal greenstone belt
UCC	Upper Continental Crust
REE	Rare earth elements
LREE	Light REE
HREE	Heavy REE
LILE	Large ion lithophile element
HFSE	High field strength element
CIA	Chemical index of alteration
PIA	Plagioclase index of alteration
ICV	Index of compositional variability
BIF	Banded iron formations
TTG	Tonalite-trondhjemite-granodiorite
CITZ	Central Indian Tectonic Zone
XRF	X-ray Fluorescence Spectrometer

✉ M. E. A. Mondal
erfan.mondal@gmail.com; meamondal@myamu.ac.in

Hamidullah Wani
wani79@gmail.com

Iftikhar Ahmad
iftikhar@myamu.ac.in

[1] Department of Geology, Government Degree College for Women Pulwama, Exchange Road, Pulwama, Jammu and Kashmir 192301, India

[2] Department of Geology, Aligarh Muslim University, Aligarh, Uttar Pradesh 202002, India

ICP-MS Inductively coupled plasma mass spectrometer
∑REE Total rare earth elements

1 Introduction

Precambrian greenstone belts are archives of the Earth's early lithospheric history (DeWit and Ashwal 1995); hence, their study is important for understanding the crust-mantle processes, and the tectonic settings that were prevalent in the Precambrian. Besides their tectonic significance, greenstone belts are also economically important as a repository for syngenetic mineralization, and epigenetic deposits (Gally et al. 2007). The greenstone belts have complex geological histories, where rocks belonging to multiple tectonic histories occur in close association with one another. The greenstone belts are made up of interlayered volcanic ultramafic–mafic rocks (komatiites, komatiitic basalts, and tholeiites) that constitute 10%–50% of the belt; and sedimentary rocks (turbidites, graywackes, meta-argillites, quartzites, cherts, and banded iron formations, which are intruded by tonalite-trondhjemite-granodiorite plutonic rocks (TTG) (DeWit and Ashwal 1995; Hunter and Stowe 1997). The greenstone belts are generally metamorphosed to greenschist to amphibolite facies and are strongly folded and sheared (Bedard et al 2013). The origin of greenstone basins remains unclear, but it is believed that magmatism had played a major role in their evolution (DeWit and Ashwal 1995; Hunter and Stowe 1997). However, it is not certain whether this magmatism was plate tectonic driven or plate independent. According to Condie (1981) and De Witt and Ashwal (1995), greenstone belts are zones of variably metamorphosed ultramafic to mafic, some also felsic volcanic rock sequences with associated sedimentary rocks that occur within Archean and Proterozoic cratons between granite and gneiss bodies. Those supracrustal rocks have been interpreted as having formed at ancient oceanic spreading centers and island arcs. These belts are a relict witness of the early Earth crustal history, and each belt has its own geological, structural, and stratigraphic characteristics, but all are economically important due to their Au, Cu, Zn, and Pb potential wealth. The Indian peninsula contains several greenstone belts, thus providing the opportunity to understand their evolution. The paper seeks the comparison of the geochemistry of meta-sedimentary rocks that occur in the Sonakhan and Mahakoshal greenstone belts of neighboring cratons of the Central Indian Shield to understand whether their origin is similar or not. The metaclastic sediments of the greenstone belts across the world, especially in the Indian peninsula have not been studied in detail and compared to unravel the mechanism of their genesis. The Indian peninsula contains several Precambrian greenstone belts. Those belts have the potential to enhance the global database on the Precambrian greenstone development, and to provide valuable information regarding their provenances, weathering history, and paleogeography. The geochemistry of the clastic rocks of the greenstone belts has not been studied as much as that of volcanic rocks to understand their genesis. In this paper, an attempt has been made to compare the geochemistry of the clastic metasedimentary rocks of the Late Archean to the Early Paleoproterozoic Sonakhan greenstone belt (hereinafter referred to as SGB) of the Bastar craton and the Late Paleoproterozoic Mahakoshal greenstone belt (hereinafter referred to as MGB) of the Bundelkhand craton to understand the origin and evolution (Fig. 1). Geochemistry and mineralogy of clastic rocks have been applied to determine the compositions of the rocks in the source area (Taylor and McLennan 1985, McLennan et al.1993; Wani and Mondal 2010; Balestra et al. 2019; Corrado et al. 2019),

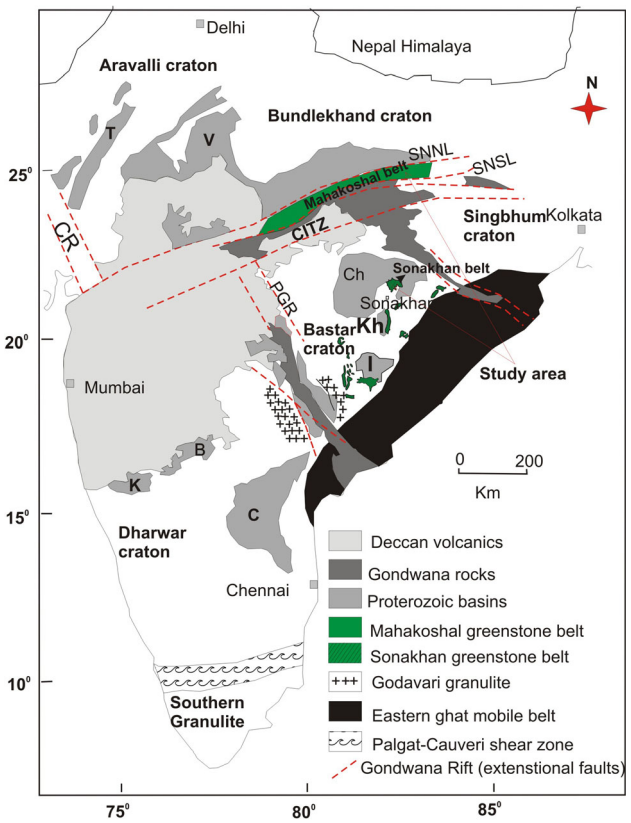

Fig. 1 Map showing the distribution of the Proterozoic basins including the Mahakoshal and Sonakhan greenstone belts on the Indian craton. Proterozoic basins shown are: Ampani (A), Bhima (B), Cuddapah (C), Chattisgarh (Ch), Indravati (I), Kaladgi (K), Khariar (Kh), Pranhita–Godavari (PG), and Vindhyan (V). CITZ = Central Indian Tectonic Zone; NNSL = North Narmada-Son Lineament (Fault); SNSL = South Narmada-Son Lineament (Fault); PGR-Pranhita–Godavari rift; CR-Cambay rift; MR-Mahanadi rift

infer the paleoclimate and weathering processes that affected the continental landmasses (Nesbitt and Young 1982; Fedo et al. 1995; Aldega et al. 2020), evaluate the secondary processes such as hydraulic sorting (McLennan et al.1993), delineate the tectonic setting of the sedimentary basin (Bhatia 1983; Bhatia and Crook 1986; Wani and Mondal 2011) and trace the evolutionary history of crust and mantle (Condie 1993).

2 Geological setting

The Central Indian shield is the amalgamation between the northerly Bundelkhand block and the southerly Bastar block, which are separated by the east–west trending Narmada-Son lineament or Central Indian Tectonic Zone (CITZ) (Fig. 1). The SGB, which occurs in the Bastar craton, covers an area of about 1200 km^2 extending NNW-SSE for about 40 km from Sonakhan (21°23′35″ N, 82°48′55″ E) in the north, to Remra (21°17′ N: 82°46′ E) in the south, and having a maximum width of 40 km in the central part (Fig. 1). The Sonakhan Group (SGB) comprises a bimodal volcanic-sedimentary sequence that unconformably overlies the basement gneissic complex locally known as the Baya Gneiss. In the north and east, the entire greenstone succession is covered by the Meso-Neoproterozoic Chhattisgarh Basin. The Sonakhan Group has been divided, from base to top into three formations (Das et al. 1990): (1) Baghmara Formation, (2) Arjuni Formation, and (3) Bilari Formation (Fig. 2, Table 1). The Baghmara Formation consists dominantly of meta-ultramafites, meta-basalt, metagabbro, pyroclastics of intermediate to basic composition, ignimbrite, rhyolite, acid tuff, pebbly tremolite-actinolite schist, and banded iron formation. In the Baghmara Formation, larger bodies of sills trending NW–SE occur. The Arjuni Formation constitutes a thick sedimentary pile interspersed with minor volcanics and overlies the Baghmara Formation. The polymictic conglomerate member of the Arjuni Formation is called the Jonk conglomerate (Das et al. 1990). The Jonk Conglomerate is dominantly clast-supported and has been suggested to be of fluvio-glacial origin. It contains mixtures of boulders and large-sized pebbles and blocks of granite, gneiss, acid volcanic rocks, porphyries, amphibolite, metabasalt, quartzite, vein quartz, BIF, jasper, schist, and phyllite. The overlying Bilari Formation includes both felsic and mafic intrusive and extrusive bodies, and like the Arangi mafic volcanics, meta-basalt, and pyroclastics along with rhyolite. The gneissic rocks, which form the basement for the SGB, have ages ranging from 3.5 to 2.6 Ga (Sarkar et al. 1990a, b). The granitoids that intrude the gneisses and the greenstone sequence yielded ages ranging from 2.6 to 1.5 Ga (Sarkar et al. 1990a). Thus, the SGB is considered to be Late Archean to Early Paleoproterozoic in age. This inference is further supported by the stratigraphic position as the SGB is overlain by the Mesoproterozoic Chhattisgarh Supergroup (1.4-1.0 Ga; Patranabis-Deb et al. 2007; Das et al. 2009; Bickford et al. 2011).

The MGB has an ENE–WSW direction with a length of 600 km that stretches from Barmanghat to Rihand Dam (Fig. 1). In the north, the MGB is separated from the Vindhyan basin by the Son Narmada North Fault (SNNF), and its southern boundary is marked by the Son Narmada South Fault (SNSF), which separates the MGB from the Proterozoic granites of the CITZ (Ramakrishnan and Vaidyanadhan 2008). The major geological units within the CITZ include metamorphosed supracrustal belts, metamorphosed mafic and ultramafic rocks, metacarbonates, iron, and manganese formations, TTG gneisses, charnockites, and related arc magmatic suites, exhumed high-pressure and ultrahigh-temperature metamorphic belts, and post-collisional K-rich granites (Acharyya 2003; Bhandari et al. 2011). The close association of metamorphosed mafic and ultramafic rocks, together with belts of iron and manganese formations in the CITZ, suggests a typical subduction–accretion setting where the Bastar

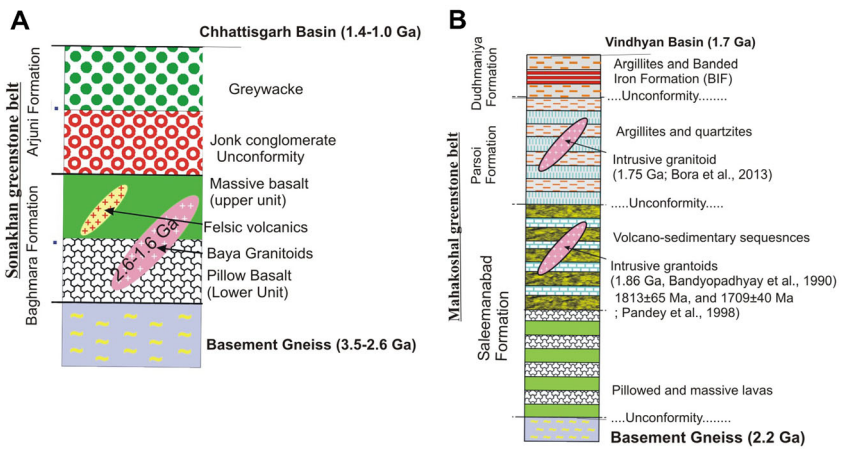

Fig. 2 Stratigraphic columns of Sonakhan and Mahakoshal greenstone belts

Table 1 Stratigraphic succession of the Sonakhan greenstone belt (Saha et al. 2000)

Unit	Description	Intrusive
Arjuni Formation	Thick succession of immature sandstone, polymictic conglomerate, brown shale/mudstone	Granophyre bodies and dioritic dykes
	Unconformity	
Baghmara Formation	Pillowed metabasalt, massive basalt with minor banded iron formation, greywacke, black shale and chert	Dykes or sills of felsic porphyry or diorite

Baya Gneiss (Basement Gneissic Complex)

craton is believed to have been subducted under the hinterland of Bundlekhand craton similar to those described from present-day active continental margins (Nakagawa et al. 2009). MGB is made up dominantly of quartzites, carbonatites, chert, banded iron formations, greywacke–argillite, and mafic volcanic rocks. The regional metamorphic grade of MGB rocks is generally between greenschist to amphibolite facies (P = 8 kPa, T = 520 °C; Deshmukh et al. 2017). The belt is divided, from base to top, into three distinct units: the Saleemanabad Formation, Parsoi Formation, and Dudhmaniya Formation (Roy and Devarajan 2000; Fig. 2; Table 2). The mafic–ultramafic and alkaline igneous rocks that are exposed in the MGB are intruded within the Saleemanabad Formation. However, the Parsoi and the Dudhmaniya formations do not contain intrusive rocks. The MGB has been affected by three phases of deformation with an overall ENE–WSW trend. The first phase is characterized by upright isoclinal folds with steep southward dipping axial planes and occurred between 1800 and 1900 Ma (Deshmukh et al. 2017). The second phase occurred between 1700 and 1800 Ma and shows vertical to inclined, E–W striking folds with axial planes dipping to the south and a pronounced crenulation cleavage (Deshmukh et al. 2017). The third phase occurred between 1700 and 1600 Ma and is marked by broad folds and N–S striking axial planes (Ramakrishnan and Vaidyanadhan 2008; Deshmukh et al. 2017). The duration of each was about 100 Ma. The granitic rocks of the TTG complex yield Rb–Sr ages up to ca. 2200 Ma (Sarkar et al. 1995). Since the TTG complex is the basement for the MGB, therefore, its supracrustals and intrusions are younger than 2200 Ma. The intrusive granites like the Jhigradandi pluton and the granitoids present in the eastern part of the MGB have been dated between 1813 ± 65 and 1709 ± 40 Ma (Pandey et al. 1998). Hence, the MGB is considered to be Late Palaeoproterozoic in age.

3 Methodology

Twenty-six fine to medium-grained metaclastic rock samples, consisting of eleven from the SGB and fifteen from the MGB were selected for major, trace, and rare earth

Table 2 Stratigraphy of the Mahakoshal greenstone belt (Roy and Devarajan 2000)

Formation/ intrusives	Saleemanabad area	Chitrangi-Gurahar- Pahar area
Intrusives	Quartz porphyry, quartz reefs, mafic dykes	Gold bearing quartz—carbonate veins, quartz reefs dolerite. Granite Granodiorite-intrusive plutonic belt along the southern margin. Jhigrandandi granite and equivalents. Lamprophyre and syenite in Sidhi
Dudhamaniya Formation	Not exposed	Alternating sequence of BIF (mixed oxide-sulphide-silicate facies) and phyllite
		.....gradational contact.....
Parsoi Formation	Dominantly phyllite with bands of greywacke, quartz wacke, quartz arenite and basalt polymictic conglomerate	Dominantly phyllite with bands of greywacke, quartz wacke, quartz arenite. Occasional presence of carbonaceous phyllite -Amsi Jiyawan fault-
	-Unconformable contact-	
Saleemanabad Formation	Mostly carbonates (stromatolitic at many places) with bands of bedded and massive chert, rare manganiferous chert, BIF, quartz arenite and metabsalt in the upper part, ultramafic (dunite) dyke	Upper part, ultramafic (dunite) dyke lower part, massive and bedded chert, BHJ, highly carbonated and fragmented metabasalt with pillows and suspected pahoehoe toes, BIF, thin argillites. Ultramafic plugs
	.....Sidhi Basement Gneissic Complex.....	
	(Gneiss complex associated with mafic, ultramafic rocks and metasediments)	

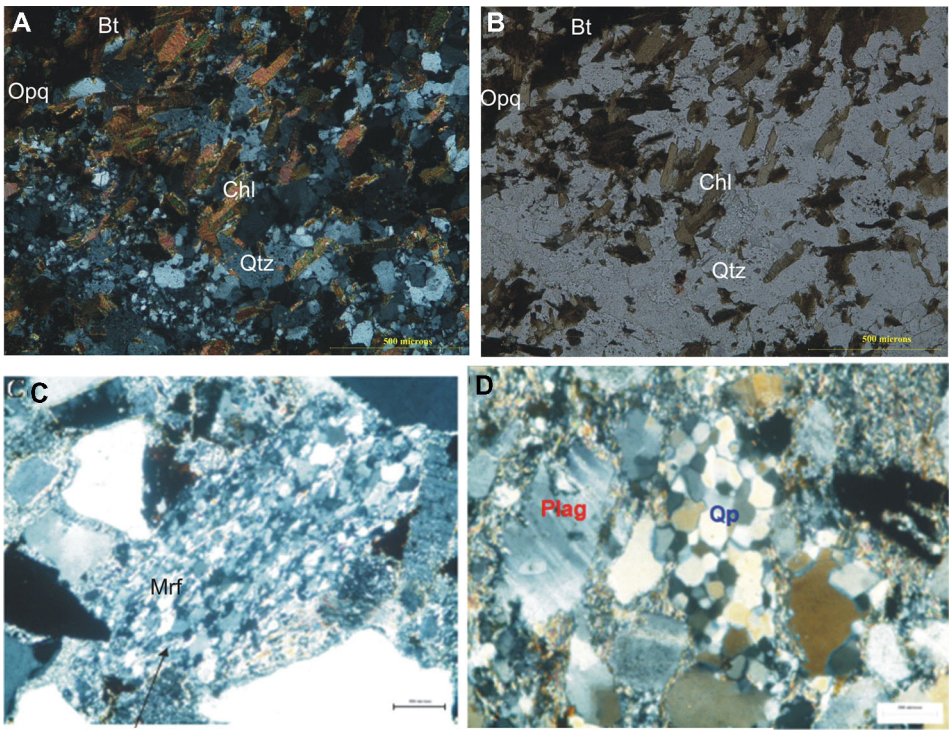

Fig. 3 Photomicrographs of Sonakhan and Mahakoshal samples **a** and **b** Mahakoshal samples show minerals of greenschist to amphibolites facies. **c** Sonkahan samples showing well-preserved plagioclase grains **d** Sonkahan samples showing the presence of metamorphic rock fragments. Qtz-quartz, Plag-plagioclase, Qp-polycrystalline quartz, Chl-chlorite, Bt-biotite, Opq-opaques, Mrf-metamorphic rock fragment

element analysis. Approximately 1 kg of each fresh rock sample was crushed and pulverized to a fine powder (200 mesh size) in an agate mill. Major elements of the SGB samples were analyzed on SIEMENS-SRS-3000 sequential X-Ray Fluorescence Spectrometer (XRF) on fused discs and fixed with polyvinyl alcohol at the Wadia Institute of Himalayan Geology (WIHG), Dehra Dun, India. The major elements of the MGB samples were analyzed on a Philips Magi XPRO PW2440, using pressed powder discs pasted with polyvinyl alcohol at the National Geophysical Research Institute (NGRI), Hyderabad, and calculated in weight percent (wt.%). Details of the analytical techniques along with precision and accuracy are described by Saini et al. (1998). Trace elements including rare earth elements (REE) of both the MGB and SGB samples were analyzed at the National Geophysical Research Institute (NGRI), Hyderabad by inductively coupled plasma mass spectrometer (ICP-MS, Perkin Elmer SCIEXELAN DRC II) and calculated in ppm (parts per million). Details of the analytical techniques along with precision and accuracy are described by Roy et al. (2007). The analytical precision and accuracy of the major oxide data are better than 1.5%. The precisions achieved for ICP-MS analyses were $< 5\%$ Relative Standard Deviation with comparable levels of accuracy. International standards were used for calibration and testing accuracy. In this study, we have synthesized the major and trace element data of the metasedimentary samples from the studies by Wani and Mondal (2016) and Mondal et al. (2018) in addition to new data.

4 Results

4.1 Mineralogy

Since the MGB rocks have undergone greenschist to amphibolite facies metamorphism, therefore, they do not reflect the original mineralogy of the studied samples. The metaclastic rocks of MGB are composed of quartz, chlorite, biotite, epidote, and opaque phases (Fig. 3a, b). The SGB metaclastic rocks are composed of quartz, chlorite, and muscovite. However, some of the samples contain well-preserved original minerals. These samples are arkosic and contain clasts of quartz, fresh plagioclase, and a few rock fragments of metamorphic origin. The plagioclase grains make up about 20% of the rock (Fig. 3c, d).

4.2 Major element geochemistry

The major elements and trace elements including the rare earth elements (REEs) data of the samples are given in Table 3. The major element composition of the SGB and MGB samples is quite variable. In general, samples of the MGB are characterized by lower mean concentrations of CaO (0.54 wt.%) and Na_2O (0.18 wt.%), and higher

Table 3 Major and trace elements of SGB and MGB samples

SGB samples													
	J-715*	J-716*	A-739	A-741	A-742	A-743	S-754	809	810	811	844	Mean	STDEV
SiO_2	51.86	51.75	69.04	72.45	70.44	65.93	65.73	68.68	71.58	71.1	71.95	66.41	7.2
Al_2O_3	15.2	15.68	16	14.54	13.77	15.77	16	15.96	17.04	15.67	14.9	15.5	0.83
$Fe_2O_3^t$	6.03	6.01	3.21	2.52	5.17	5.7	4.83	3.63	3	2.95	2.55	4.14	1.34
MnO	0.1	0.09	0.02	0.03	0.06	0.06	0.04	0.09	0.04	0.02	0.02	0.05	0.02
MgO	1.93	1.75	1.3	0.87	1.09	1.39	4.1	1.41	0.75	0.66	1.33	1.5	0.9
CaO	1.7	1.6	1	1.64	2.1	0.4	0.43	3.38	0.14	1.22	1.47	1.37	0.86
Na_2O	2.54	2.39	1.85	2.98	2.76	2.58	2.98	2.56	1.31	3.37	2.16	2.49	0.54
K_2O	3.91	4.06	4.69	3.64	2.69	4.36	3.38	2.88	3.97	2.96	3.43	3.63	0.6
TiO_2	0.8	0.8	0.31	0.33	0.36	0.5	0.54	0.34	0.3	0.3	0.26	0.44	0.18
P_2O_5	0.65	0.5	0.07	0.06	0.08	0.1	0.16	0.07	0.06	0.08	0.06	0.17	0.19
Trace elements in ppm													
Sc	12.17	13.21	4.82	4.67	5.2	8.62	8.59	5.77	6.22	4.95	6.43	7.33	2.84
V	92.82	99.96	27.44	26.41	30.87	48	15.96	40.94	30.09	37.27	28.2	43.45	26.22
Cr	17.13	17.66	18.84	18.5	20.06	30.9	9.5	28.89	25.48	27.07	26.29	21.85	6.08
Co	20.51	24.34	12.69	23.44	20.82	23.35	5.61	17.05	14.06	20.11	11.46	17.59	5.68
Ni	12.61	13.03	9.18	7.78	10.99	13.48	7.18	6.99	9.79	8.31	7.01	9.67	2.37
Rb	108.8	117.2	156.6	117.5	88.83	136	135.7	104.1	145.9	88.25	138.9	121.6	21.78
Sr	243.1	226	80.14	129	106.2	101.9	65.71	159.3	63.42	494	118.1	162.4	119.2
Y	20.78	21.43	41.71	35.25	47.42	47.43	42.49	24.96	24.38	7.98	26.39	30.93	12.17
Zr	522.3	551.7	842.3	760.3	1052	723	1199	491	481	247	427.4	663.6	270.7
Nb	8.53	9.07	17.98	16.74	18.15	21.14	13.95	14.76	18.83	6.94	15.95	14.73	4.44
Cs	4.28	4.69	3.67	3	2.39	4.86	3.39	2.96	3.75	4.38	3.14	3.68	0.75
Ba	512	564	619	462	418	610	659	496	761	823	763	608	126
Hf	14.06	14.54	24.65	21.96	29.47	20.97	34.59	14.39	14.37	7.38	13.14	19.05	7.7
Ta	0.81	0.83	2.92	2.92	2.72	2.52	1.95	2.71	3.46	2.24	3.33	2.4	0.85
Th	5.27	5.45	24.9	24.29	30.08	23.73	18.6	25.73	34.38	12.73	30.63	21.4	9.39
U	1.65	1.72	25.36	11.98	9.22	6.42	5.98	7.97	9.31	1.58	13.55	8.61	6.57
Pb	7.1	7.63	9.18	40.04	13.57	13.07	10.91	9.34	3.43	2.8	2.1	10.83	9.95
La	36.13	37.03	40.06	48.16	60.67	47.61	55.05	47.8	53.98	54.02	44.91	47.76	7.48
Ce	69.64	71.77	70.03	82.94	104	85.65	101.9	83.19	90.45	94.36	78.05	84.73	11.49
Pr	8.41	8.69	7.58	8.77	10.87	9.5	11.66	8.88	10.14	10.34	8.44	9.39	1.17
Nd	31.01	32.27	25.25	28.38	35.22	32.4	40.69	29.47	33.9	34.35	28.26	31.93	3.99
Sm	5.46	5.66	5.1	5.15	6.34	6.39	7.34	5.49	6.26	4.97	5.47	5.78	0.68
Eu	1.68	1.79	1.12	1.13	1.25	1.38	1.88	1.15	1.32	1.52	1.29	1.41	0.25
Gd	4.9	5.14	5.31	5.24	6.43	6.41	7.03	5.23	5.63	4.29	5.31	5.54	0.75
Tb	0.8	0.8	1.11	0.99	1.25	1.3	1.31	0.81	0.86	0.48	0.86	0.96	0.24
Dy	4.05	4.03	6.96	6.01	7.87	8.19	7.75	4.41	4.62	1.79	4.91	5.51	1.92
Ho	0.76	0.77	1.47	1.28	1.69	1.71	1.64	0.85	0.89	0.28	0.93	1.11	0.44
Er	2.05	2.08	4.22	3.54	4.75	4.8	4.69	2.53	2.67	0.81	2.79	3.17	1.26
Tm	0.3	0.32	0.75	0.61	0.81	0.82	0.83	0.43	0.47	0.11	0.49	0.54	0.23
Yb	1.87	1.89	4.69	3.9	5.26	5.08	5.29	2.76	3.04	0.73	3.22	3.43	1.48
Lu	0.28	0.29	0.7	0.58	0.77	0.76	0.84	0.44	0.47	0.1	0.49	0.524	0.22
ICV	1.11	1.05	0.77	0.82	1.03	0.94	1.01	0.88	0.55	0.73	0.75	0.88	0.16
CIA	56.92	58.25	61.61	55.1	54.93	61.87	63.08	54.22	71.75	58.83	59.98	59.68	4.76
PIA	60.14	62.26	69.08	57.27	56.43	68.86	68.38	55.35	84.09	61.62	64.24	64.34	7.81
REE	167.3	172.5	174.4	196.7	247.2	212	247.9	193.4	214.7	208.2	185.4	201.8	27.67

Table 3 continued

SGB samples													
	J-715*	J-716*	A-739	A-741	A-742	A-743	S-754	809	810	811	844	Mean	STDEV
LREE/HREE	9	9.05	5.61	7.43	7.2	5.95	6.92	9.36	9.72	19.53	8.12	8.07	3.78
Eu/Eu*	0.99	1.01	0.65	0.66	0.6	0.66	0.79	0.66	0.68	1.01	0.73	0.76	0.16
(La/Yb)n	13.83	14	6.12	8.84	8.26	6.71	7.45	12.38	12.7	53.01	9.98	9.97	13.26
(Gd/Yb)n	2.16	2.24	0.93	1.11	1.01	1.04	1.09	1.56	1.53	4.85	1.36	1.33	1.13

MGB samples	M-4	M-5	M-6	M-107	M-113	M-117	M-46	M-50	M-51	M-55
SiO_2	78.2	79.1	78.8	60.7	56.06	58.2	49.45	57.99	68.26	62.98
Al_2O_3	9.55	3.9	8.05	18.2	20.71	19.1	11.9	10.4	17.5	17.52
$Fe_2O_3^t$	4.33	1.02	1.85	7.87	8.72	7.53	19.26	11.6	1.15	8.49
MnO	0.1	0.03	0.1	0.03	0.03	0.05	0.37	0.18	0.04	0.07
MgO	4.25	3.44	3.4	4.66	4.53	4.84	15.6	9.33	3.68	5.79
CaO	0.3	0.29	0.22	0.27	0.37	0.33	0.53	1.97	1.25	0.85
Na_2O	0.68	0.02	0.05	0.12	0.19	0.23	0.01	0.87	0.15	0.02
K_2O	1.01	0.72	0.84	5.4	5.7	5.73	0.22	2.97	4.88	1.43
TiO_2	0.47	0.35	0.32	0.53	0.59	0.8	1.51	1.71	0.37	1.08
P_2O_5	0.04	0.02	0.04	0.05	0.07	0.07	0.21	0.28	0.02	0.19
Trace elements in ppm										
Sc	4.4	2.9	2.5	13	12	14	19	21	5	11
V	66.5	32.8	27.3	114	102	120	202	183	58	126
Cr	66.5	42.4	35.2	92	82	100	123	137	49	118
Co	19.8	6	14.3	9	8	9	28	29	2.3	13.4
Ni	34.6	22.3	35.1	51	45	53	81	122	38	76
Rb	16.7	12.1	10.1	201	209	251	7	80	113	54
Sr	24.5	16.5	15.6	62	69	66	23	77	49	48
Y	6.8	4.3	4.1	24	21	30	17	18	26	21
Zr	597	519	417	5165	4291	5351	7587	13414	13922	14157
Nb	1.8	2.4	1.1	14	13	17	9	12	19	11
Cs	1.9	1.4	1.1	12	9	13.9	2.4	9	5	7
Ba	154	111	128	472	633	566	115	358	300	271
Hf	12.9	11	8.8	89	76	93	150	263	276	273
Ta	0.17	0.22	0.1	3	3	4	0.8	1.1	1.7	1.28
Th	3.2	2.6	2.8	17	17	24	9.6	11	35	15.2
U	0.96	0.96	0.73	4	4	4	2.5	3.4	8.3	4.9
Pb	11.3	12	8.2	29.9	29.2	31.2	19.7	21.2	33	19.3
La	11.3	6.6	12.6	35	44	58	26	27	86	21
Ce	20.6	10.5	14.2	74	93	111	54	58	158	42
Pr	2.6	1.6	3.2	7	9	12	5.7	6.2	16	4.4
Nd	9.3	5.9	11.2	28	31	44	24	24.6	59	17
Sm	1.7	1.1	1.8	5	6	8	5.1	5.3	11	4
Eu	0.45	0.29	0.39	0.98	1	1.35	1.02	1.2	0.71	0.83
Gd	1.7	1.04	1.6	4.5	5	7	4.6	4.6	8.9	3.5
Tb	0.21	0.13	0.17	0.64	0.72	0.95	0.75	0.71	1.1	0.65
Dy	1.1	0.65	0.76	3.7	3.5	5	3.6	3.4	4.8	3.6
Ho	0.19	0.12	0.12	0.91	0.81	1	0.66	0.69	0.96	0.75
Er	0.71	0.43	0.43	2.4	2.3	3.3	1.6	1.9	2.6	2
Tm	0.13	0.07	0.07	0.49	0.44	0.56	0.26	0.32	0.44	0.36

Table 3 continued

MGB samples	M-4	M-5	M-6	M-107	M-113	M-117	M-46	M-50	M-51	M-55
Yb	0.87	0.55	0.5	3	2.8	3.4	1.7	2.2	3.01	2.5
Lu	0.15	0.09	0.09	0.53	0.47	0.58	0.27	0.38	0.49	0.4
ICV	1.15	1.49	0.82	1.03	0.97	1.01	3.12	2.73	0.65	1
CIA	77.6	74.4	85.3	73.6	74.32	72.7	90.71	55.83	69.16	84.85
PIA	83.6	84.8	93.7	94.7	93.65	92.9	92.24	58.9	82.9	91
REE	51	29.1	47.1	166	200	256	129.2	136.5	353	102.9
LREE/HREE	8.25	7.62	10.4	8.68	10.73	10.1	7.93	7.86	14.34	6.05
Eu/Eu*	0.8	0.82	0.7	0.63	0.55	0.55	0.64	0.74	0.21	0.67
(La/Yb)n	9.31	8.6	18.1	8.36	11.27	12.2	10.97	8.8	20.49	6.02
(Gd/Yb)n	1.61	1.56	2.64	1.24	1.47	1.7	2.23	1.72	2.44	1.15

MGB samples	M-61	M-66	M-127	M-133	M-134	Mean	STDEV	*p*-value
SiO_2	66.96	50.89	54.5	64.73	64.81	63.44	9.61	0.404
Al_2O_3	17.61	21.75	20.4	18.79	19.31	15.6	5.42	0.921
$Fe_2O_3^t$	3.6	9.11	6.64	4.61	3.65	6.62	4.72	0.07
MnO	0.05	0.1	0.03	0.04	0.04	0.08	0.08	0.245
MgO	4.02	4.56	5.68	3.91	4.04	5.44	3.16	0.0002
CaO	0.24	0.31	0.62	0.15	0.13	0.52	0.49	0.005
Na_2O	0.13	0.11	0.05	0.08	0.1	0.18	0.24	0.013
K_2O	5.85	8.58	7.69	4.83	5.94	4.11	2.7	0.56
TiO_2	0.48	1.92	1.09	0.68	0.93	0.85	0.51	0.01
P_2O_5	0.1	0.17	0.54	0.04	0.05	0.12	0.13	0.018
Trace elements in ppm								
Sc	8	34	6.2	11	12	11.73	8.23	0.072
V	61	175	76.9	109	101	103.6	52.65	0.001
Cr	63	112	42.4	82	95	82.63	32.18	0.000002
Co	3	12	5.7	4.2	3	11.1	8.56	0.0419
Ni	36	50	33.8	69	50	53.12	25.21	0.00001
Rb	147	301	13.1	184	230	121.9	102	0.992
Sr	47	49	44.7	59	55	47.02	19.2	0.001
Y	48	50	14.6	25	30	22.65	13.5	0.128
Zr	12440	15382	3468	20957	16448	8941	6656	0.0002
Nb	16	18	7.1	11	15	11.16	5.85	0.107
Cs	6	16	5.6	7.7	6.7	6.98	4.49	0.013
Ba	548	792	646	531	599	414.9	224	0.017
Hf	243	302	60.2	409	326	172.9	132.1	0.0004
Ta	1.3	1.6	1.1	1.6	2	1.53	1.1	0.042
Th	26	26	12.9	25.6	21	16.5	9.7	0.224
U	6	5.6	3.1	7.2	5.9	4.1	2.27	0.025
Pb	23.8	35.1	31.1	21.3	34.1	24	8.7	0.001
La	58	31	51.1	52	67	39.1	22.8	0.188
Ce	122	38	101	107	137	76.03	46.49	0.497
Pr	11	7	10.4	10	14	8	4.24	0.246

Table 3 continued

MGB samples	M-61	M-66	M-127	M-133	M-134	Mean	STDEV	*p*-value
Nd	42	28	36.9	40	51	30.12	15.52	0.672
Sm	8	5.6	5.8	7.3	9	5.64	2.78	0.851
Eu	0.85	1.2	1.2	1.1	1.3	0.92	0.33	0.0005
Gd	7.5	5.2	4.9	5.9	6.9	4.85	2.24	0.287
Tb	1.2	1.02	0.5	0.81	0.86	0.69	0.32	0.032
Dy	7.4	7.1	2.6	3.8	3.7	3.64	1.96	0.026
Ho	1.6	1.8	0.57	0.9	0.79	0.79	0.47	0.092
Er	4.3	5.1	1.5	2.7	2.5	2.25	1.3	0.088
Tm	0.67	0.95	0.26	0.52	0.47	0.4	0.23	0.138
Yb	4.5	6.3	1.5	3.6	3.3	2.64	1.54	0.213
Lu	0.63	0.95	2.6	0.62	0.55	0.58	0.6	0.718
ICV	0.81	1.13	1.06	0.75	0.76	1.23	0.72	0.083
CIA	71.6	68.43	68.2	76.93	73.87	74.49	8.31	0.00002
PIA	94.54	94.36	90.9	97.1	96.98	89.48	9.58	0.0000003
REE	269.6	139.2	221	236.2	298.3	175.7	97.1	0.002
LREE/HREE	8.41	3.7	13.1	10.84	13.64	9.45	2.87	0.67
Eu/Eu*	0.33	0.67	0.68	0.51	0.5	0.53	0.16	0.01
(La/Yb)n	9.24	3.52	24.4	10.36	14.56	10.59	5.54	0.56
(Gd/Yb)n	1.37	0.68	2.7	1.35	1.72	1.51	0.57	0.98

$Eu/Eu^* = (Eu)_n/[(Sm_n \times Gd_n)]^{1/2}$; $Fe_2O_3^t$ = Total Iron; p-value means p-value obtained using Students' t-test between SGB and MGB samples; STDEV = Standard Deviation

*This study. Rest of the data from Mondal et al. (2018) and Wani and Mondal (2016)

concentrations of $Fe_2O_3^t$ (6.62 wt.%), MnO (0.08 wt.%), TiO_2 (0.85 wt.%), MgO (5.44 wt.%), K_2O (4.11 wt.%) as compared to the SGB samples (CaO = 1.37 wt.%, Na_2O = 2.49 wt.%, $Fe_2O_3^t$ = 4.14 wt.%, MnO = 0.05 wt.%, TiO_2=0.44 wt.%, MgO = 1.5 wt.%, K_2O = 3.63 wt.%; Table 3). However, the SiO_2, Al_2O_3, and P_2O_5 concentrations do not show large variations between the MGB samples (SiO_2 = 63.44, Al_2O_3 = 15.6, P_2O_5 = 0.12 wt.%) and SGB samples (SiO_2 = 66.41, Al_2O_3 = 15.5, P_2O_5 = 0.17 wt.%). The difference in major-element compositions between the MGB and SGB samples has proved to be significant for MgO, Na_2O, TiO_2, and P_2O_5 using the Student's *t*-test at better than 95% confidence level ($p < 0.05$) (Table 3).

4.3 Trace elements

The mean values of transitional elements of the MGB samples have higher concentrations of Sc (11.73 ppm), V (103.6 ppm), Cr (82.3 ppm) and Ni (53.12 ppm), but lower of Co (11.2 ppm) in comparison to SGB (Sc = 7.33 ppm, V = 43.45 ppm, Cr = 21.85 ppm, Ni = 9.67 ppm, Co = 17.59 ppm; Table 3). This difference in transition element concentrations between the MGB and SGB samples has proved to be significant for V, Cr, Ni, and Co using the Student's t-test at a better than 95% confidence level ($p < 0.05$) (Table 3). As compared to the SGB samples, the MGB samples have higher concentrations of LILEs like Cs (6.98 ppm) and Pb (24 ppm) but have lower of Sr (47.02 ppm), Ba (414.9 ppm), Th (16.5 ppm), and U (4.1 ppm). The Rb (121.9 ppm) concentrations are almost similar between the SGB and the MGB samples. HFSEs such as Zr (8941 ppm) and Hf (172.9 ppm) concentrations are higher in the MGB samples while Y (22.65 ppm), Nb (11.16 ppm), and Ta (1.53 ppm) are lower. The difference in LILEs and HFSEs between the SGB and the MGB samples has proved to be significant for Sr, Cs, Ba, U, Pb, Zr, Hf, and Ta using the Student's *t*-test at better than 95% confidence level ($p < 0.05$) (Table 3).

4.4 Rare earth elements (REE)

The total rare earth elements ($\sum$REE) concentration in the samples from the SGB have a higher mean value (201.8 ppm) and a lower mean value in the MGB samples (175.7 ppm). On the chondrite normalized REE diagram

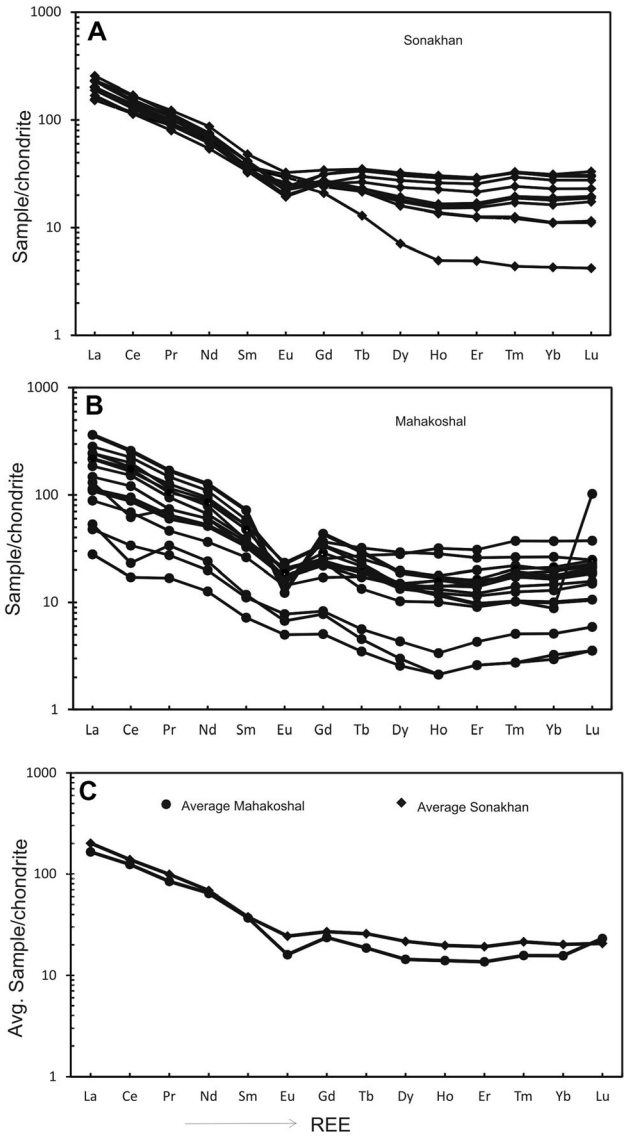

Fig. 4 Chondrite normalized REE diagram (Sun and McDonough 1989) for the Sonakhan samples, Mahakoshal samples, and average of Sonakhan and Mahakoshal samples

(Fig. 4; normalizing values from Sun and McDonough (1989), the LREE patterns of the SGB and the MGB samples are fractionated with LREE enrichment (La/Yb)n = 9.97 for the SGB samples and 10.59 for the MGB samples, flat HREE (Gd/Yb)n = 1.33 for the SGB and 1.51 for the MGB samples. The samples from both belts have a negative Eu/Eu* anomaly, which is 0.76 for the SGB and 0.53 for the MGB samples. Overall the concentrations of REE of the SGB and MGB samples are almost similar. However, a difference for Eu, Tb, and Dy has proved to be significant using the Student's *t*-test at better than 95% confidence level ($p < 0.05$) (Table 3).

5 Discussion

5.1 Source rock characteristics

In comparison to Upper Continental Crust (UCC) (Taylor and McLennan 1985), samples of the MGB are rich in MgO and $Fe_2O_3^t$, and Co, Sc, V, Ni, and Cr (Fig. 5). The major elements as MgO, $Fe_2O_3^t$, and compatible elements, such as transition elements are characteristic of mafic source rocks (Feng and Kerrich, 1990). The proportions of mafic elements, especially MgO, $Fe_2O_3^t$, Ni, and Cr, indicate the presence of olivine and pyroxene in the source rocks. This is evident from the significant correlation between MgO and $Fe_2O_3^t$ (r = 0.89). In comparison to UCC, the SGB samples do not have a high concentration of these mafic elements (except for Co) (Fig. 5). The difference in mafic components between the MGB and SGB samples is consistent with the Student's *t*-test which has proved to be significant (> 95%) for MgO, V, Cr, Ni, and Co (Table 3).

On the UCC-normalized diagram, both the MGB and SGB samples are rich in Th and U. However, in terms of HFSEs such as Nb and Ta, SGB samples show slightly higher concentration, while MGB samples show depletion (prominent negative anomalies) in these elements. The enrichment of LILEs and depletion of HFSEs, especially in Nb and Tb, are associated with arc rocks, hence, indicating an arc character for the source of MGB samples (Eissen et al. 1991; Fig. 5). Both the MGB and SGB samples show slight LREE and HREE enrichment in comparison to UCC, indicating a source similar to UCC (Fig. 6). This is further attested by the strong LREE enrichment [(La/Yb)n = 9.97 in the SGB samples and 10.59 in the MGB samples], and slight HREE enrichment on the chondrite normalized REE diagrams [(Gd/Yb)n = 1.33 of the SGB and 1.51 of the MGB samples]. Furthermore, both the SGB and MGB samples show a significant negative Eu anomaly (Eu/Eu* = 0.76 for the SGB and 0.53 for the MGB). It is interesting to note that the REE patterns and Eu anomalies of the MGB and SGB samples are similar to each other and suggest that the same mineral phases control REE in both groups of samples derived from highly differentiated sources such as granites. However, from the foregoing discussion, it becomes clear that the MGB samples also carry a mafic signature given by the amounts of $Fe_2O_3^t$, MgO, Ni, Cr, Co, and V. The samples also show an arc signature given by their high concentrations in LILEs and depletion in HFSEs. Therefore, it can be considered that the MGB received the clastic load from a mixed source of arc affinity with a major contribution from mafic rocks and less from felsic rocks, whereas the clastic load of the SGB derived from a felsic source only. The preservation of a

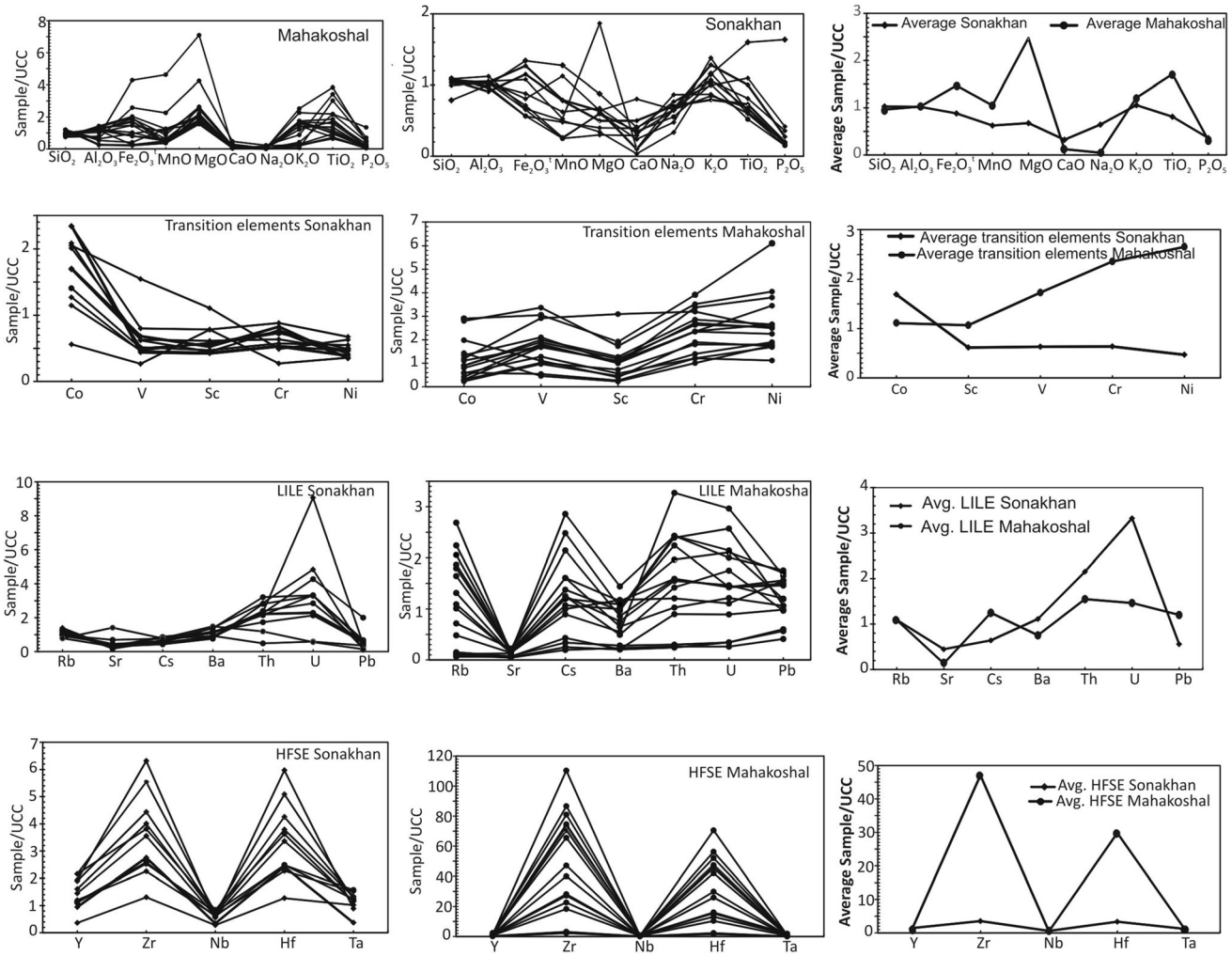

Fig. 5 UCC normalized (Taylor and McLennan 1985) major and trace element diagrams for Sonakhan samples Mahakoshal samples, and average of the Sonakhan and Mahakoshal samples

felsic signature rather than a mafic signature in the MGB samples reflected by REE characteristics is actually because their budget in clastic sedimentary rocks is chiefly controlled by granitoids, which mask the contribution of mafic–ultramafic components (Jahn and Condie 1995). This conclusion is consistent with the enrichment of both Cr and Zr in the MGB samples since these two elements monitor chromite and zircon contents, respectively (Wronkiewicz and Condie 1989). The difference between Cr and Zr concentration of SGB and MGB samples is also depicted by the Student's *t*-test at > 95% confidence level ($p < 0.05$). The MGB samples are enriched in both Cr and Zr (82.63 and 8941 ppm), in comparison to the SGB ones (Cr = 21.85 ppm and Zr = 663.6 ppm). On the Ni–Cr diagram (Taylor and McLennan 1985; Fig. 7), the MGB and SGB samples plot along a linear trend. It is evident from Fig. 7 that the SGB samples, which plot at the lower end of the Ni–Cr trend (post-Archean field) may have been derived from a felsic source, while the clastic load of the MGB is enriched in both Ni and Cr in comparison to the SGB one's plot at the upper end of the Ni–Cr trend (Post Archean to Neoarchean field). This complements the enrichment of MgO and $Fe_2O_3^t$ in the MGB samples, which reflects the mafic nature of source rocks.

5.2 Classification of SGB and MGB sediments and sedimentary sorting

To classify the terrigenous sands, Pettijohn et al. (1972) developed a diagram based on log (Na_2O/K_2O) versus log (SiO_2/Al_2O_3) (Fig. 8A). According to this classification, the samples of the MGB are mostly litharenites while the ones of the SGB are greywackes, which indicates a compositional immaturity of the sediments. The proportions of the major elements of the MGB and SGB samples reflect the relative proportions of quartz to feldspars and

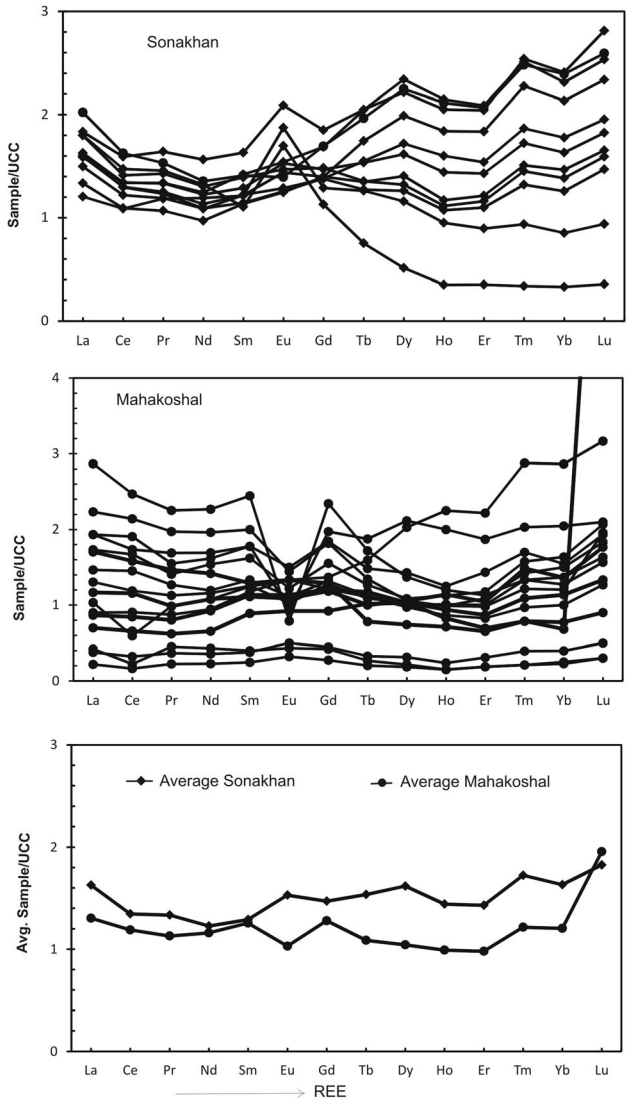

Fig. 6 UCC normalized (Taylor and McLennan 1985) REE (rare earth elements) for the Sonakhan samples Mahakoshal samples, and average of the Sonakhan and Mahakoshal samples

clays/phyllosilicates, and the majority of the samples plot along the expected mixing trend on the SiO_2 versus Al_2O_3 plot (Fig. 8b). Furthermore, the plot of SiO_2 versus Al_2O_3 (Fig. 8b) can better be used to understand the effect of weathering and sedimentary sorting. It is clear from the plot that the SGB samples (except two samples) cluster in the middle of the trend line indicating a compositional homogeneity with a small effect of weathering and sorting. However, the MGB samples which plot all along a linear trend, indicate that most of the samples were affected by weathering and only three samples with SiO_2 value $> 72\%$ have been affected by sorting.

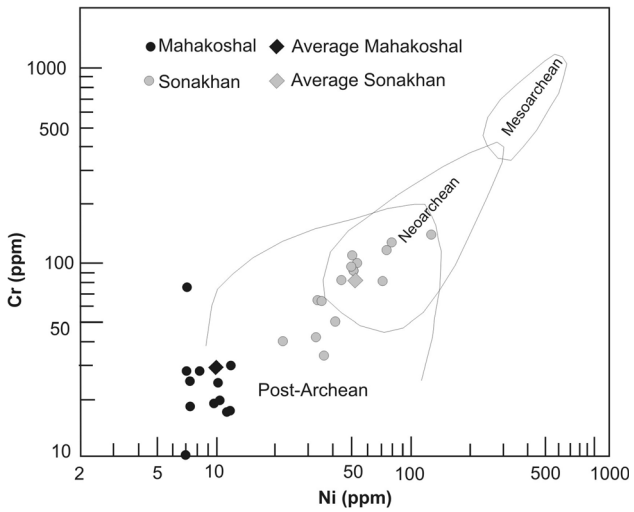

Fig. 7 Ni–Cr distributions in the Sonakhan and Mahakoshal samples (after Taylor and McLennan 1985)

5.3 Sediment recycling and tectonics

The Index of Compositional Variability, ICV = $(Fe_2O_3 + K_2O + Na_2O + CaO + MgO + TiO_2)/ Al_2O_3$ can be used to evaluate the original composition of the sediments (Cox and Lowe 1995; Cox et al. 1995; Mondal et al. 2012). The ICV is a measure of the abundance of alumina relative to other major constituents of rock except for SiO_2. Non-clay minerals have a higher ratio of the major cations to Al_2O_3 than clay minerals. Thus the non-clay minerals have a higher ICV. The ICV value decreases in the order of pyroxene and amphibole (10–100), biotite (8), alkali feldspar (0.8–1), plagioclase (0.6), muscovite and illite (0.3), montmorillionite (0.15–0.3), and kaolinite (0.03–0.05) (Cox et al. 1995). Hence, immature shales with a high percent of non-clay silicate minerals show ICV values greater than one. These shales are often found in tectonically active settings as first-cycle deposits (Van de Kamp and Leake 1985). In contrast, more mature mudrocks with mostly clay minerals generally have ICV values lower than one (Cox et al. 1995). Such shales ought to form in cratons of quiescent tectonic environments (Weaver 1989). However, they have also been found as the first cycle material in intensely weathered zones (Barshad 1966). The ICV values of the SGB samples range from 0.55 to 1.11 with an average of 0.88 suggesting that most of the samples are compositionally mature and were likely dominated by recycling, but this is not the case. Since these samples are greywacke which is texturally and compositionally immature rocks, and, therefore, the reasons for having low ICV values must be different. The petrographic evidence shows that some of the samples have preserved the original

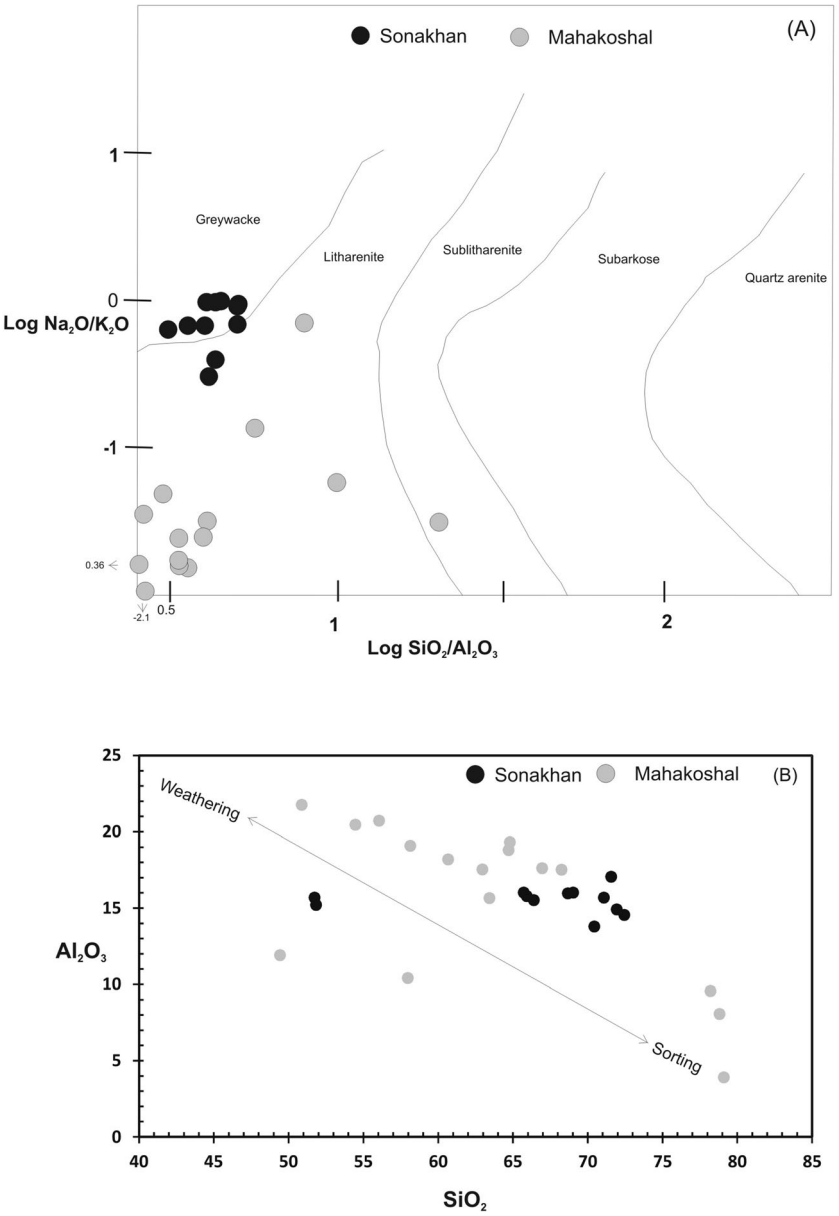

Fig. 8 **a** Sandstone classification of the Sonakhan and Mahakoshal samples using log (SiO_2/Al_2O_3) versus log (Na_2O/K_2O) (Pettijohn et al. 1973). **b** A plot of SiO_2 versus Al_2O_3 to understand the effect of weathering and sedimentary sorting

mineralogy and contain abundant fresh plagioclase grains (up to 20%) therefore, lowering their ICV values to ≤ 1 (Fig. 3). Furthermore, the presence of abundant plagioclase grains in the metagreywackes indicates that these rocks are arkosic. There are also some metamorphic rock fragments in these metagreywackes. The rock fragments are formed by continental block faulting of basement rocks (Dickinson 1985). The fresh nature of plagioclase grains suggests that the source rocks were not affected by severe chemical weathering. The ICV value of MGB samples shows a wide variation ranging from 0.65 to 3.1 with an average value of 1.24 and was dominated by first cycle sediments of mafic sources and, therefore, indicate tectonically active settings of the basin. This inference is further supported by the litharenite nature of the MGB samples. Dickinson (1985) reported that the litharenites derived from orogens, where stratified rocks are deformed, uplifted and eroded, and deposited in a foreland basin. According to Dickinson (1985), litharenites are also formed during back-arc thrusting where the arcs are uplifted and eroded. Since the Central Indian Tectonic Zone, suggests a typical subduction–accretion setting where the Bastar craton is believed to have been subducted under the hinterland of the Bundlekhand craton, therefore, such inference can be taken into consideration. The abundance of the trace elements as Sc, La, Zr, Cr, Th is characteristic for different tectonic

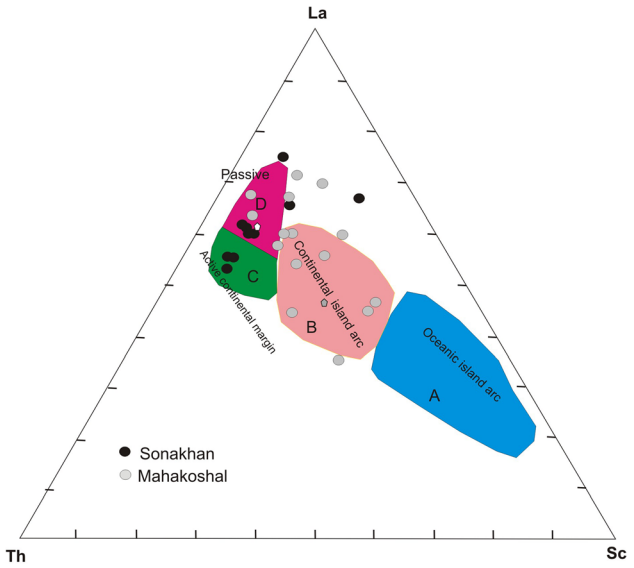

Fig. 9 Th–La–Sc trace element tectonic setting discrimination plot for the Sonakhan and Mahakoshal samples (after Bhatia and Crook 1986)

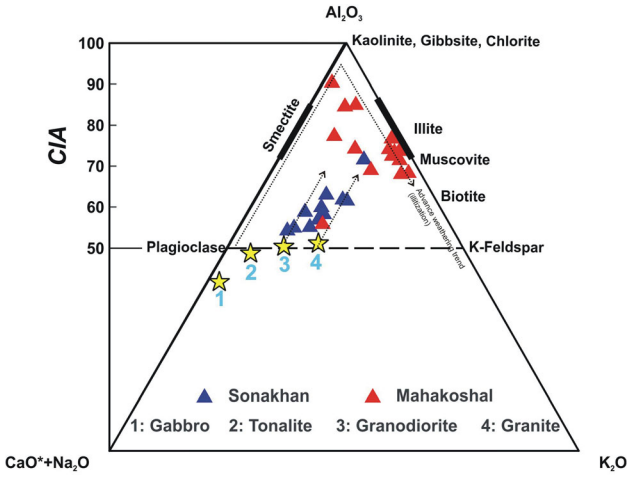

Fig. 10 Al_2O_3–(CaO^* + Na_2O)–K_2O (A–CN–K) ternary plot, after Nesbitt and Young (1982) (CaO^* = CaO in silicate phase) shows the weathering trends of Sonakhan and Mahakoshal samples and their probable source rocks. Numbers 1–4 denote compositional trends of initial weathering profiles of different rocks. 1—gabbro; 2—tonalite; 3—granodiorite; 4—granite

settings and is considered to remain unaffected by remobilization during weathering, as well as medium-grade metamorphic processes (Bhatia and Crook 1986). Therefore, these elements have a great significance to decipher the source rock composition and tectonic setting. The ternary plot of La-Th-Sc (Bhatia and crook 1986; Fig. 9) can depict four types of tectonic settings, namely (a) oceanic arcs, (b) continental arcs, (c) active continental margin, and (d) passive continental margin. The results on this diagram indicate a continental arc provenance for the

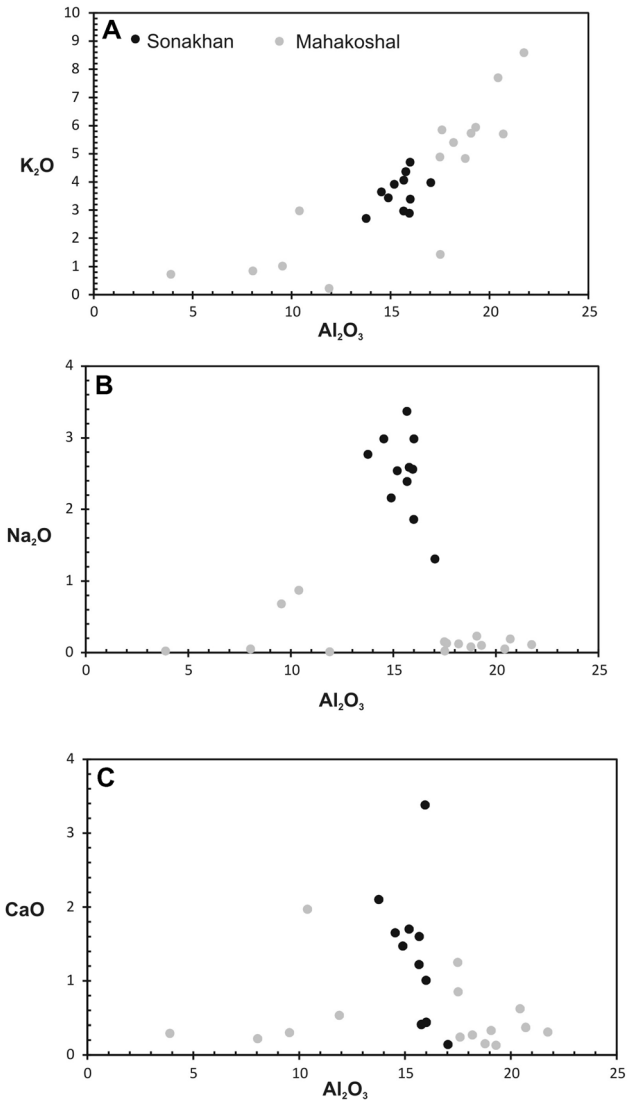

Fig. 11 Bivariate diagrams showing correlation between (**a**) Al_2O_3 and K_2O (**b**) Al_2O_3 and Na_2O and (**c**) Al_2O_3 and CaO

MGB samples and a continental passive and active margin provenance for the SGB samples (Fig. 9).

5.4 Paleoweathering and paleoweathering trends

It is clear from the UCC normalized diagrams that, almost for the same values of SiO_2, Al_2O_3, and Rb, the MGB samples have higher values of immobile elements like TiO_2, and lower values of Na_2O, CaO, and Sr than the SGB samples. This suggests that the MGB samples underwent an intenser degree of chemical weathering than the SGB samples (Table 3). Nesbitt and Young (1982) defined a chemical index of alteration (CIA) to quantitatively measure the degree of weathering (in molecular proportions): $CIA = [Al_2O_3/(Al_2O_3 + CaO^* + Na_2O + K_2O)] \times 100$; where CaO^* represents the CaO in the silicate fraction only

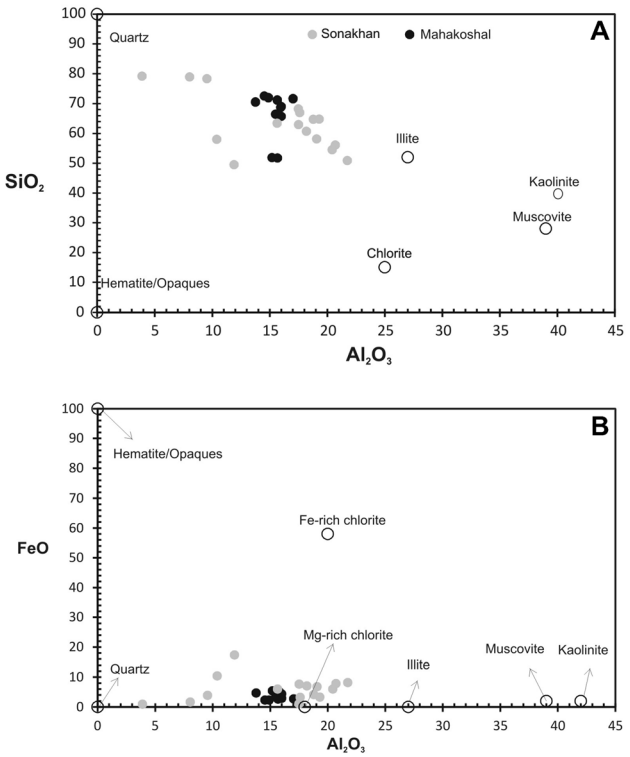

Fig. 12 Bivariate plots showing (**a**) SiO_2 versus Al_2O_3 concentrations and (**b**) Al_2O_3 versus FeO concentrations. The Sonakhan and Mahakoshal samples have been plotted relative to the idealized composition of the observed minerals (Cullers and Podkovyrov 2000)

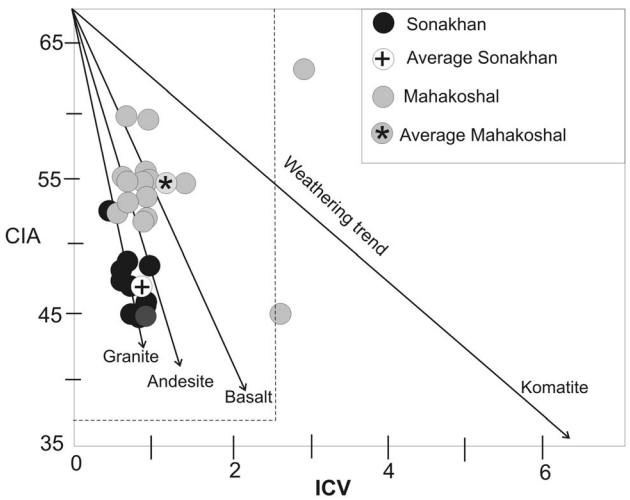

Fig. 13 Weathering trends of the Sonakhan and Mahakoshal samples on the Index of Compositional Variability (ICV) versus Chemical Index of Alteration (CIA) plot (Potter et al. 2005)

(Nesbitt and Young 1982). The average CIA values of the SGB samples vary from 54.22 to 71.75 with an average of 59.8 indicating a low to moderate chemical weathering. The CIA values of the MGB samples have a wide range of CIA values and range from 55.83 to 90.71 with an average of 74.50 suggesting moderate to intense chemical weathering. Moderate to intense weathering of the source area for the MGB samples and low to moderate chemical weathering for the SGB samples is further indicated by plagioclase index of alteration (PIA) values (Table 3) given by the following equation: PIA = $[(Al_2O_3–K_2O)/(Al_2O_3 + CaO + Na_2O–K_2O)] \times 100$, proposed by Fedo et al. (1995). The MGB samples have PIA values of 58.9–97.1 with an average of 89.4 indicating near-complete alteration of plagioclase. However, the SGB samples have a PIA value in the range of 54.93–71.75 with an average of 64.34 suggesting very low weathering of plagioclases.

Another approach to understanding the weathering trend of the original source rock is to plot molar ratios of Al_2O_3–$(CaO^* + Na_2O)$–K_2O in A–CN–K compositional space to potentially separate compositional changes of sediments related to chemical weathering, transportation, diagenesis, and metamorphism (Fedo et al. 1995, 1997; Fig. 10). The A-CN-K diagram is useful for evaluating fresh rock compositions and examining their weathering trends because the upper crust is dominated by plagioclase and K-feldspar–rich rocks and their weathering products, the clay minerals (Nesbitt and Young 1984, 1989). Normally sediments show weathering trends that plot parallel to the A–CN boundary, and they extract back to a plagioclase–alkali feldspar horizontal line of the source composition unless post-depositional K-metasomatism affected the rocks (Fig. 10). The K-metasomatism of kaolinite weathered rocks can produce illite, which plots at right angles to the A–K side of the diagram (Fig. 10). Chemical weathering reactions involving the destruction of plagioclase drive these trends to more aluminous or potassic compositions along the A–K join (Nesbitt and Young 1989). The predicted weathering trends of the SGB and the MGB samples in relation to probable source rocks of granite, granodiorite, diorite, tonalite, and basalt compositions are shown in Fig. 8. The CIA values of the SGB samples vary from 54.22 to 71.75 with an average of 69.68 indicating a low to moderate chemical weathering and pointing to the availability of a weakly weathered profile available for erosion in the source area. The SGB samples plot on a trend reflecting a predominantly granitic to a granodioritic source. This trend reflects alteration of K-feldspar to illite, and samples that plot to the right of the granodiorite and granite trend indicate that some minor addition of K has occurred.

In comparison to SGB, the MGB samples that plot in the A–CN–K diagram produce no clear trend back to the source composition. It is clear from the diagram that most of the MGB samples neither plot parallel to the A-CN boundary nor perpendicular to the A-K side of the diagram, but show an advanced weathering trend in which the samples plot along the A–K line suggestive of intense chemical weathering of the source rocks ranging in

composition from tonalite to basalt (Fig. 10). However, the samples show a wide range of CIA values from 55.83 to 90.71 (average = 74.50) and the anomalously low contents of Na_2O that range from 0.01 to 0.87 wt.% (average = 0.18), whereas K_2O is high and ranges from 0.22 to 7.69 wt.% (average = 4.11) suggesting that post-depositional K-metasomatism has affected these rocks (Table 3). This is further supported by a positive correlation coefficient value between Al_2O_3 and K_2O (r = 0.85) and, negative correlation between Al_2O_3 and Na_2O (r = − 0.27) and Al_2O_3 and CaO (− 0.14) (Fig. 11). Potassium metasomatism is particularly common in the Precambrian rocks, and typically involves the conversion of kaolin (residual weathering product) to illite by reaction with K-bearing pore waters during diagenesis (Fedo et al. 1995). Such a trend is most likely produced by intense weathering of mafic rocks, which were later affected by post-depositional K-metasomatism. This interpretation is consistent with other major and trace element characteristics, which indicate the mafic source rocks for the MGB samples as already discussed. An estimate of premetasomatized or 'corrected' CIA values can be made by drawing a line from the K_2O apex through individual data points; the intersection point of this line with the 'predicted weathering path' gives the pre-metasomatized CIA value, which can be directly read off the scale on the left. The difference between the pre-metasomatized and the current CIA values allows quantitative estimation of K enrichment in a rock. The present CIA values (uncorrected) range from 55.83 to 90.71 with an average value of 74.50. Since these sediments have undergone K metasomatism, the pre-metasomatised CIA values must have been quite higher. The corrected pre-metasomatised CIA values of the MGB samples have been calculated and fall in the range of 66–97.5, with an average of 90.1 indicating near-complete destruction of plagioclases. This is consistent with the PIA values of these samples. Therefore, CIA and PIA values suggest moderate to intense chemical weathering of the source area.

In another attempt to characterize weathering of the source rocks, Cox et al. (1995) have observed that the K_2O/Al_2O_3 ratios are useful in depicting how much alkali feldspar vs. plagioclase and clay minerals may have been present in the original sediments. The K_2O/Al_2O_3 ratios of different K and Al-bearing minerals vary significantly, for example, K_2O/Al_2O_3 ratios of alkali feldspar = ∼0.4–1, illite = ∼0.3, and for other clay minerals = ∼0. Shales with K_2O/Al_2O_3 ratios greater than 0.5 suggest a significant quantity of alkali feldspar relative to other minerals in the original sediments. The K_2O/Al_2O_3 ratios of the MGB samples vary from 0.01 to 0.29 with an average of 0.26, suggesting minimal alkali feldspar relative to other minerals. The K_2O/Al_2O_3 ratios of the SGB samples vary from 0.18 to 0.29 with an average of 0.23. This in turn implies that alkali feldspar should have been minimal in the source rocks. This is further revealed on the SiO_2 versus Al_2O_3 concentrations and Al_2O_3 versus FeO concentrations of samples which have been plotted relative to the idealized composition of the observed minerals (Fig. 12). It is clear from the SiO_2 versus Al_2O_3 plot that most of the samples plot between quartz and illite composition. However, four samples two from each the MGB and SGB are skewed towards hematite and opaques. On the Al_2O_3 versus FeO plot the samples plot between quartz and Mg-rich chlorite and between Mg-chlorite and illite indicating the presence of both illite and Mg-chlorites in the original sediments. However, a few samples are skewed towards Fe-rich chlorite. The occurrence of illite is very well in agreement with the A-CN-K diagram in which the samples plot near the illite field.

Another method of extracting information on weathering trends of the source rocks from major element data of clastic rocks that show the influence of chemical weathering is to pair the CIA value with the ICV (index of chemical variability) (Gaschnig et al. 2016; Fig. 13). ICV values are high for mafic source lithologies and when plotted against CIA values (Fig. 13), straight lines connecting a completely weathered end member to average igneous compositions reflect weathering trends (Potter et al. 2005), on this plot the MGB samples cluster on the weathering trend of granite, while the majority of the MGB samples plot on a broad weathering trend between andesite and basalt-komatiite with an average basaltic protolith, which is consistent with other geochemical signatures indicating contrasting source rocks available for SGB during the Late Archean to Early Paleoproterozoic and for the MGB during the Late Paleoproterozoic in the Central Indian Shield.

6 Implications

6.1 Implications for greenstone belt development

Based on the summary of geochemistry from the SGB and MGB of the Central Indian Shield as discussed above, it is reasonable to envisage that the greenstone belt formation during the Late Archean and Late Paleoproterozoic in the central Indian shield involved two different mechanisms. The Late Archean to Early Paleoproterozoc SGB reveals that the basin received most of its sediments from highly differentiated rocks (granitic) like that of a craton with a passive-active tectonic setting and therefore, appears to have been developed as an autochthnous greenstone belt. The study of Mondal and Raza (2009) using geochemical data of volcanic rocks of the SGB reveals that the

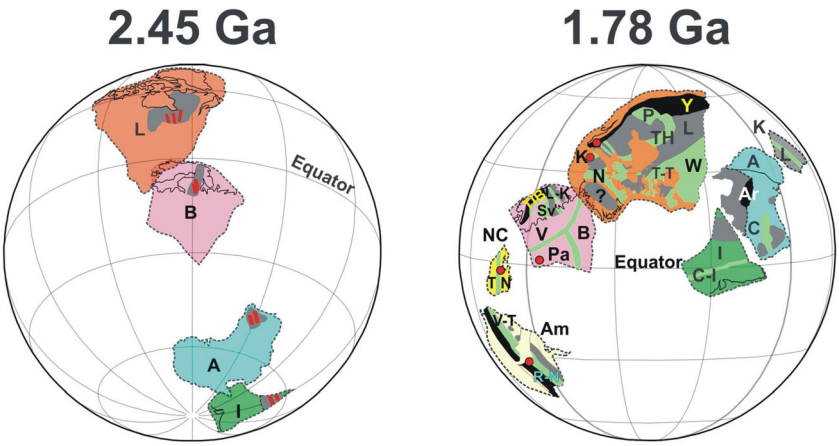

Fig. 14 Figures showing the position of India in the configuration of 2.45 Ga Columbia supercontinent and 1.78 Ga Rodina Supercontinent (Pesonen et al. 2003)

Sonakhan greenstone belt of the Bastar craton evolved by mantle-plume upwelling. Several pieces of evidence show, that mantle plumes may have played a role in Archean magma production, crustal underplating, and development of Archean greenstone belts (Tomlinson and Condie 2001). The relative abundance of plume-related greenstones in the Archean may reflect the hotter, less easily subducted Archean oceanic lithosphere as compared to the Proterozoic (Tomlinson and Condie 2001). In contrast to the SGB, the Late Paleoproterozoic MGB shows a robust geochemical signature of bimodal source rocks with subduction signature and continental arc setting and therefore, appears to have been developed as near continental arc systems as an allochthonous greenstone belt, similar to those observed in younger orogens. Arc rocks in greenstone belts occur mainly in the bimodal geochemical association in both the basaltic basal zones of these sequences and in the isolated felsic eruptive centers (Ayer et al. 2005). Since the MGB is present in the Central Indian Tectonic Zone, which has very well-developed fold and thrust belts, metamorphic core complexes, blue schists, and, therefore, should be considered as an allochthonous greenstone belt. Therefore, SGB and MGB record both vertical (mantle plume related) and lateral accretionary tectonics (plate subduction-related), building continents in the early Earth in India as seen in other parts of the world (VanKranendonk et al. 2004, Santosh 2013). Furthermore, the geochemical signatures of the sedimentary record of the SGB and MGB are not consistent with an Archaean upper crust dominated by the bimodal basic-felsic suite with both units derived by melting at mantle depths and the Proterozoic upper continental crust dominated by K-rich granites, derived by intracrustal melting. Therefore, revealing a reverse of the typical age-composition relations, that is, the occurrence of bimodal basic-felsic suite in the Late Paleoproterozoic MGB sediments and felsic in the Late Archean to Early Paleoproterozoic SGB sediments. Such compositional trend can be interpreted in terms of tectonic differences between the SGB and MGB as revealed in the present study. This does not pose any problem to the general understanding of the worldwide secular change in crustal composition from bimodal in the Archean to felsic in the Proterozoic. This contrast between the typical age-composition relations has been identified in many places of the world and has been attributed to the tectonic difference by McLennan and Taylor (1988).

6.2 Implications for paleogeography

Studying weathering regimes of the Precambrian rocks is important for a better understanding of the influence of climate on weathering, erosion, and runoff in the geological past. The high chemical weathering inferred from the Late Paleoproterozoic MGB can be attributed to weathering under moderate to severe environmental conditions such as low pH, high temperature and humidity, and extreme leaching typical of tropical climatic conditions. However, the CIA values of the Late Archean to Early Paleoproterozoic SGB indicate chemical weathering under cool conditions. The change in CIA values from the Late Archean to the Late Paleoproterozoic in the Central Indian Shield can be interpreted either by a change in the global climate from the Late Archean to the Late Paleoproterozoic or due to the migration of the Central Indian Shield through various climatic zones. The latter interpretation seems to be more accurate since the paleomagnetic studies of the Late Archean rocks indicate that the Indian plate was set at higher latitudes during the Late Archean to Early Paleoproterozoic (at 2.45 Ga) while in low latitudes during the later part of the Paleoproterozoic (1.78 Ga). The Paleomagnetic data used for reconstruction at 2.45 Ga reveals that the Ur fragments Yilgarn from Australia and especially Dharwar from India, was placed at high, almost polar (south) latitudes (Pesonen et al. 2003). These Late Archean to Early Paleoproterozoic supracrustal strata have been considered similar to Neoproterozoic strata that also have

glaciogenic sequences and paleoweathering zones (e.g., Evans 2000). It is interesting to note that the Jonk Conglomerate of the SGB also suggests its fluvio-glacial origin (Das et al 1990). Good quality palaeomagnetic data at 1.78 Ga from Amazonia, Australia, Baltica, India, Kalahari, Laurentia, and North China (Fig. 14) reveals that the 1.78 Ga "Early Columbia" is made of two landmasses: the one consists of an elongate large continental area of Amazonia, Baltica, Laurentia, and North China, and another includes Australia, India, and Kalahari. These continents were positioned at low to intermediate latitudes during 1.88–1.77 Ga (Pesonen et al. 2003). Thus, the variation in the CIA values from the Late Archean to the Late Paleoproterozoic in the Central Indian Shield is the result of the migration of the Indian plate from southern high to lower latitudes, and the results of this study are very much consistent with the paleomagnetic data and the paleographic positions that were placed for India in the configurations for supercontinents (Fig. 14).

7 Conclusions

The origin of greenstone belts remains unclear and there is an intense debate regarding their origin. The Indian Peninsula posses a number of greenstone belts providing a great opportunity to understand their development. Based on the geochemical study of metasedimenatry sequences from the SGB and MGB of the Central Indian Shield, it is concluded that those greenstone formations involved two entirely different mechanisms that evolved from Late Archean to Late Paleoproterozoic and recorded both vertical (plume related rift) and lateral accretionary tectonics (subduction-related). The Late Archean to Early Paleoproterozoc SGB developed as an autochthonous greenstone belt and received most of its sediments from highly differentiated continental rocks in a passive-active tectonic setting like that of a continental rift. The Late Paleoproterozoic MGB developed as an allochthonous greenstone belt, similar to those in younger orogens, and received sediments from continental arc-related bimodal sources. The variation in the CIA values from the Late Archean to the Late Paleoproterozoic is due to the migration of the Indian plate from southern high latitudes to lower latitudes. This is very much consistent with the paleomagnetic data and paleographic positions of India in the supercontinent configurations.

Acknowledgements We wish to express sincere thanks to the Director of National Geophysical Research Institute (NGRI), Hyderabad, and the Director of Wadia Institute of Himalayan Geology, Dehra Dun for providing laboratory facilities during chemical analysis. We are thankful to the Chairperson, Department of Geology, A.M.U., India for providing the necessary facilities to carry out this investigation. H. Wani thankfully acknowledges the financial support of UGC, Govt. of India in the form of a research project F. No. 40-304/2011 (SR). We also thank three anonymous reviewers for their suggestions and critical reviews.

Author contributions Data acquisition: HW, MEAM. Conception: MEAM, IA. Writing/Drafting: HW, IA. Data interpretation: HW, MEAM, IA. Revision: MEAM, IA. All authors read and approved the final manuscript.

Funding HW acknowledges the financial support from UGC, Govt. of India in the form of a research project F. No. 40-304/2011(SR). MEAM is thankful to the Department of Science and Technology, Govt. of India for financial support in the form of a Research Project (SR/S4/ES-180/2005).

Data availability All data generated and analyzed during this study are included in this published article and its supplementary information files.

Declarations

Conflict of interest The authors declare that they have no competing interests.

References

Acharyya SK (2003) The nature of mesoproterozoic Central Indian tectonic zone with exhumed and reworked older granulites. Gondwana Res 6(2):197–214. https://doi.org/10.1016/S1342-937X(05)70970-9

Aldega L, Brandano M, Cornacchia I (2020) Trophism, climate and paleoweathering conditions across the Eocene-Oligocene transition in the Massignano section (Northern Apennine, Italy). Sed Geol 405(3–4):10570

Ayer J, Thurston PC, Bateman R, Dube B, Gibson HL, Hamilton MA, Hathway B, Hocker SM, Houle M, Hudak GJ, Ispolatov V, Lafrance B, Lesher CM, MacDonald PJ, Peloquin AS, Piercey SJ, Reed LE, Thompson PH (2005) Overview of results from the Greenstone architecture project: discover Abitibi initiative, Ontario Geological Survey, Open File Report 5984, 125 p

Balestra M, Corrado S, Aldega L, Morticelli MG, Sulli A, Sassi W (2019) Thermal and structural modeling of the Scillato wedge-top basin source-to-sink system: insights into the Sicilian fold-and-thrust belt evolution (Italy). Geol Soc Am Bull 131(11–12):1763

Bedard JH, Harris LB, Thurston PC (2013) The Hunting of the snArc. Precambrian Res 229:20–48

Bershad I (1966) The effect of a variation in a precipitation on the nature of a clay mineral formation in soils from acid and basic igneous rocks. In: Proceedings international clay conference

Bhandari A, Pant NC, Bhowmik SK, Goswami S (2011) ~1.6 Ga ultrahigh-temperature granulite metamorphism in the Central Indian Tectonic Zone: insights from metamorphic reaction history geothermobarometry and monazite chemical ages. Geol J 46(2–3):198–216. https://doi.org/10.1002/gj.1221

Bhatia MR (1983) Plate tectonics and geochemical composition of sandstones. J Geol 91:611–627

Bhatia MR, Crook KAW (1986) Trace element characteristics of greywackes and tectonic discrimination of sedimentary basins. Contrib Mineral Petrol 92:181–193

Bickford ME, Basu A, Patranabis-Deb S, Dhang PC, Schieber J (2011) Depositional history of the Chhattisgarh basin, Central

India: Constraints from new SHRIMP zircon ages. The J Geol 119(1):33–50
Bora S, Kumar S, Yi K, Kim N, Lee TH (2013) Geochemistry and U-Pb SHRIMP zircon chronology of granitoids and microgranular enclaves from Jhirgadandi Pluton of Mahakoshal Belt, Central India Tectonic Zone, India. J Asian Earth Sci 70–71(1):99–114
Condie KC (1993) Chemical composition and evolution of the upper continental crust: contrasting results from surface samples and shales. Chem Geol 104:1–37
Condie KC (1981) Archean greenstone belts. Developments in Precambrian Geology. Elsevier Scientific Publishing Company 3, 440p
Corrado S, Aldega L, Perri F, Critelli S, Muto F, Schito F, Tripodi F (2018) Detecting syn-orogenic extension and sediment provenance of the Cilento wedge top basin (southern Apennines, Italy): mineralogy and geochemistry of fine-grained sediments and petrography of dispersed organic matter. Tectonophysics 750:404–418
Cox R, Lowe DR (1995) Compositional evolution of coarse clastic sediments in the southwestern United States. J Sediment Res 65:477–494
Cox R, Low DR, Cullers RL (1995) The influence of sediment recycling and basement composition on evolution of mudrock chemistry in the southwestern United States. Geochemi Cosmochimi Acta 59:2919–2940
Cullers RL, Podkovyrov VN (2000) Geochemistry of the Mesoproterozoic Lakhandashales in southeastern Yakutia, Russia: implications for mineralogical and provenance control, and recycling. Precambr Res 104:77–93
Das N, Roy Burman KJ, Vatsa US, Mahurkar YV, Dhoundial DP (1990) Sonakhan schist belt: a Precambrian granite–greenstone complex. Geol Surv India Special Pub Ser 28:118–132
Das K, Yokoyama K, Chakraborty PP, Sarkar A (2009) Basal tuffs and contemporaneity of the Chhattisgarh and Khariar Basins based on new dates and geochemistry. J Geol 117:88–102
Deshmukh T, Naraga P, Bhattacharya A, Madhavan K (2017) Late Paleoproterozoic clockwise P-T history in the Mahakoshal Belt, Central Indian Tectonic Zone: implications for Columbia supercontinent assembly. Precam Res 298:56–78
Dickinson WR (1985) Interpreting provenance relations from detrital modes of sandstones. In: Zuffa GG (ed) Provenance of arenites. D. Reidel Publications Co., Dordrecht, pp 333–362
Weaver CE (1989) Clays, muds and shales. Elsevier
Eissen JP, Lefevre C, Maillet P, Morvan G, Nohara M (1991) Petrology and Geochemistry of the central North Fiji Basin spreading centre (southwest Pacific) between 16°S and 22°S. Mar Geol 98:201–239
Evans DAD (2000) Stratigraphic, geochronological, and paleomagnetic constraints upon the Neoproterozoic climatic paradox. Am J Sci 300:347–433
Fedo CM, Young GM, Nesbitt HW (1997) Paleoclimatic control on the composition on the Paleoproterozoic Serpent Formation, Huronian Supergroup, Canada: a greenhouse to icehouse transition. Precam Res 86:211–223
Fedo CM, Nesbitt HW, Young GM (1995) Unraveling the effects of potassium metasomatism in sedimentary rocks and paleosols, with implications for weathering conditions and provenance. Geology 23:921–924
Feng R, Kerrich R (1990) Geochemistry of fine grained clastic sediments in the Archean Abitibi greenstone belt, Canada: Implications for provenance and tectonic setting. Geochimi Cosmochimi Acta 54:1061–1081
Galley AG, Syme R, Bailes A (2007) Metallogeny of the Paleoproterozoic Flin Flon belt, Manitoba and Saskatchewan. In: Goodfellow W (ed) Mineral deposits of Canada: a synthesis of major deposit-types, District Metallogeny, the evolution of geological provinces, and exploration methods: geological associaton of Canada, Mineral Deposits Division, Special Publication 5, pp 509–531
Gaschnig RM, Rudnick RL, McDonough WF, Kaufman AJ, Valley JW, Zhaochu H, Gao S, Beck ML (2016) Compositional evolution of the upper continental crust through time, as constrained by ancient glacial diamictites. Geochimi et Cosmochimi Acta 186(2016):316–343
Herron MM (1988) Geochemical classification of terrigenous sands and shales from core or log data. J Sediment Petrol 58(5):820–829
Hower J, Eslinger E, Hower ME, Perry EA (1976) Mechanism of burial metamorphism of argillaceous sediment: 1. Mineralogical and chemical evidence. Geol Soc Am Bull 87(5):725–737
Hunter DR, Stowe CW (1997) A historical review of the origin, composition, and setting of Archaean Greenstone Belts (pré-1980). In: De-Wit M, Ashwal LD (eds) Greenstone belts. Oxfords
Jahn BM, Condie KC (1995) Evolution of the Kaapvaal Craton as viewed from geochemical and Sm–Nd isotopic analyses of intracratonic pelites. Geochimi Cosmochimi Acta 59:2239–2258
McLennan SM (1989) Rare earth elements in sedimentary rocks: Influence of provenance and sedimentary process. Rev Mineral 21:169–200
McLennan SM, Taylor SR (1988) Crustal evolution: Comments on "The Archean- Proterozoic transition: Evidence from the geochemistry of metasedimentary rocks from Guyana and Montana" by A. K. Gibbs, C. W. Montgomery, P. A. O'day and E. A. Erslev. Geochimi Cosmochim Acta 52(3):785–787
McLennan SM, Hemming S, McDaniel DK, Hanson GN (1993) Geochemical approaches to sedimentation, provenance and tectonics. In: Johnsson MJ, Basu A (eds) Processes controlling the composition of clastic sediments: geological Society of America Special Paper 284, pp 21–40
Mondal MEA, Wani H, Mondal B (2012) Geochemical signature of provenance, tectonic setting and chemical weathering in the Quaternary flood plain sediments of the Hindon river, Gangetic plain, India. Tectonophysics 566–567(2012):87–94
Mondal B, Hussain MF, Mondal MEA (2018) Geochemistry of Paleoproterozoic metasedimentary rocks from Sonakhan greenstone belt, north-east Bastar Craton, central Indian shield: implications for provenance, paleoweathering and tectonic setting. J Appl Geochem 20:325–343
Mondal MEA, Raza M (2009) Tectonomagmatic evolution of the Bastar craton of Indian shield through plume-arc interaction: evidence from geochemistry of the mafic and felsic volcanic rocks of Sonakhan greenstone belt. 32, paper 7. In: Talat A, Francis H, Punya C (Eds.) Geological Anatomy of India and the Middle East, 2009
Nakagawa M, Santosh M, Maruyama S (2009) Distribution and mineral assemblages of bedded manganese deposits in Shikoku Southwest Japan: implications for accretion tectonics. Gondwana Res 16(3-4):609–621. https://doi.org/10.1016/j.gr.2009.05.003
Nesbitt HW, Young GM (1982) Early Proterozoic climates and plate motions inferred from major element chemistry of lutites. Nature 54:2015–2050
Nesbitt HW, Young GM (1984) Prediction of some weathering trends of plutonic and volcanic rocks based on thermodynamic and kinetic consideration. Geochimica et Cosmochimica Acta. 48:1523–1534
Nesbitt HW, Young GM (1989) Formation and diagenesis of weathering profiles. J Geol 97:129–147
Patranabis-Deb S, Bickford ME, Hill B, Chaudhuri AK, Basu A (2007) SHRIMP ages of zircon in the uppermost tuff in

Chattisgarh basin in the Central India ~500-Ma adjustment in Indian Proterozoic stratigraphy. J Geol 115:407–415

Pesonen LJ, Elming S-Å, Mertanen S, Pisarevsky S, D'Agrella-Filho MS, Meert JG, Schmidt PW, Abrahamsen N, Bylund G (2003) Palaeomagnetic configuration of continents during the Proterozoic. Tectonophysics 375:289–324

Pandey BK, Krishna V, Chabria T (1998) An overview of Chotanagpur Gneiss-Granulite Complex and adjoining sedimentary sequences, eastern and Central India. International Seminar on Precambrian Crust in Eastern and Central India 1998, pp. 131–135 Abstract Volume UNESCO-IUGS-IGCP-368

Pettijohn FJ, Potter PE, Siever R (1972) Sand and Sandstone. Springer Verlag, Berlin

Pettijohn FJ, Potter PE, Siever R (1973) Sand and sandstone. Springer-Verlag, Berlin

Potter PE, Maynard JB, Depetris PJ (2005) Mud and mudstones: introduction and overview. Springer, Heidelberg, p 297

Ramakrishnan M, Vaidyanadhan R (2008) Geology of India, vol I. Geological Society of India, Bangalore

Santosh M (2013) Evolution of continents, cratons and supercontinents: Building the habitable Earth. Curr Sci 104(7):871–879

Roy P, Balaram V, Kumar A, Satyanarayanan M, Rao G (2007) New REE and trace elementdata on two international kimberlitic reference materials by ICP-MS. J Geostandards Geoanal Res 31:261–273

Roy A, Devarajan MK (2000) A reappraisal of the stratigraphy and tectonics of the Paleoproterozoic Mahakoshal supracrustal belt, Central India Geological Survey of India. Spec Publ 57:79–97

Saini NK, Mukherjee PK, Rathi MS, Khanna PP, Purohit KK (1998) A new geochemical reference sample of granite (DG-H) from Dalhousie, Himachal Himalaya. J Geol Soc India 52:603–606

Saha D, Deb GK, Dutta S (2000) Granite-greenstone relationship in the Sonakhan belt, Raipur district, Central India. Geol Surv India Spec Publ 57:67–78

Sun SS, McDonough WF (1989) Chemical and isotopic systematics of oceanic basalts: implications for mantle composition and processes. In: Saunder AD, Norry MJ (eds) Magmatism in oceanic basins. Geological Society London Special Publication, pp 313–345

Sarkar A, Sarkar G, Paul DK, Mitra ND (1990a) Precambrian geochronology of the central Indian shield: a review. Geol Soc India Special Pub 28:453–482

Sarkar G, Paul DK, deLaeter JR, McNaughton NJ, Mishra VP (1990b) A geochemical and Pb, Sr isotopic study of the evolution of granite gneisses from the Bastar craton. Central India J Geol Soc India 35:480–496

Sarkar A, Paul DK, Potts PJ (1995) Geochronology and geochemistry of the mid-Archaean trondhjemitic gneiss from the Bundelkhand Craton, Central India. In: Saha AK (ed) Recent Researches in Geology 16. Hindustan Publishing Corporation, pp 76–92

Taylor SR, McLennan SM (1985) The continental crust: its composition and its evolution. Blackwell, Oxford, p 312

Tomlinson KY, Condie KC (2001) Archean mantle plumes: evidence from greenstone belt geochemistry. Geol Soc Am Special Paper 352:341–357

Van der Kamp PC, Leake BE (1985) Petrography and geochemistry of feldspathic and mafic sediments of the northeastern Pacific margin. Trans R Soc Edinburgh Earth Sci 76:411–449

Van Kranendonk MJ, Collins WJ, Hickman AH, Pawley MJ (2004) Critical tests of vertical vs horizontal tectonic models for the Archaean East Pilbara Granite-Greenstone Terrane, Pilbara Craton, Western Australia. Precambrian Res 131:173–211

Wani H, Mondal MEA (2010) Petrological and geochemical evidence of the Paleoproterozoic and the Meso-Neoproterozoic sedimentary rocks of the Bastar craton, Indian Peninsula: implications on paleoweathering and Proterozoic crustal evolution. J Asian Earth Sci 38:220–232

Wani H, Mondal MEA (2011) Evaluation of provenance, tectonic setting, and paleoredox conditions of the Mesoproterozoic-Neoproterozoic basins of the Bastar craton, Central Indian Shield: Using petrography of sandstones and geochemistry of shales. Lithosphere 3(2):143–154

Wani H, Mondal MEA (2016) Geochemical evidence for the Paleoproterozoic arc-back arc basin association and its importance in understanding the evolution of the central Indian Tectonic Zone. Tectonophysics 690:318–335

Wit De, Ashwal (1995) Greenstone belts: what are they? S Afr J Geol 98(4):505–520

Wronkiewicz DJ, Condie KC (1989) Geochemistry and provenance of sediments from the Pongola Supergroup, South Africa: evidence from a 3.0 Ga-old continental craton. Geochim Cosmochim Acta 53:1537–1549